Progress In Electromagnetics Research C, Vol. 84, 1–9, 2018

A Preliminary Research on Skull Healing Utilizing Short Pulsed Radar Technique on Layered Cranial Surgery Phantom Models

Doojin Lee[1], Jacob Velander[2], Daniel Nowinski[3], and Robin Augustine[2, *]

Abstract—This paper presents a novel approach of sensing the defect response after craniotomy on cranial surgery phantom models utilizing a short pulsed radar technique. The proposed antenna has demonstrated that the short pulse can be radiated without antenna's own distortion, which is a desirable characteristic for sensing defect response. The layered microwave head phantom has been developed for the purpose of emulating the healing stages of cranial surgery after craniotomy. The fabricated phantom has been validated with reference values reported in literature. The longitudinal scan has been performed for various skull thicknesses as a preliminary study. The one-dimensional pulsed profile has been obtained to achieve the pulse compression so that the defect response can be highlighted. The results obtained in this paper have the potential that the microwave based technique can be utilized for monitoring the healing stages for the future work.

1. INTRODUCTION

Craniotomy is a medical terminology, and it is performed on skull layer to temporally remove a piece of skull to have access to the brain for surgical issues [1–4]. The surgical issues involved in craniotomy are blood clots inside the vessel, tumors inside the brain, and brain trauma caused by an accident, etc. [1, 2]. Above and beyond these, the craniotomy is also performed for craniosynostosis treatment. The craniosynostosis is a congenital disorder in infants in which one or more of suture lines have prematurely fused on skull layer before the brain has fully grown [1–4]. Here, depending on which suture lines have fused earlier, the craniosynostosis can be grouped such as sagittal synostosis, coronal synostosis, metopic synostosis, and lambdoid synostosis [3]. Due to fused suture lines, the intracranial pressure is increased resulting in abnormal head shape in the end. The increased intracranial pressure also develops other complications such as visual impairment, developmental disability, etc. If one affects the optic nerve, it leads to visual impairment. The developmental disability is caused once the intracranial pressure has an effect on brain area. In this respect, craniotomy is performed to reduce the increased intracranial pressure and to provide enough void to fused suture lines gradually.

After craniotomy, monitoring the healing stages during post treatment care is a very important issue to ensure proper medical intervention when needed [1, 3]. In this regard the medical equipment has been tried to make a follow-up on post treatment care such as X-ray, computed tomography (CT), and even magnetic resonance imaging (MRI). However, X-ray can only visualize the quantity of callus formation, so it is not a possible way to use for follow-up after craniotomy [1, 4, 5]. Besides, it radiates high-ionizing radiation; therefore, infants are highly vulnerable to it. CT scans and MRI equipment are very powerful and accurate; however, they also use high ionizing radiation and expensive. Therefore, they cannot be used for follow-up which results in difficulties in follow-up after craniotomy [1–4, 6].

Received 26 February 2018, Accepted 8 April 2018, Scheduled 28 April 2018

* Corresponding author: Robin Augustine (Robin.Augustine@Angstrom.uu.se).

[1] Mechanical and Mechatronics Engineering,University of Waterloo (UW), Waterloo, ON, Canada. [2] Department of Engineering Sciences, Microwaves in Medical Engineering Group, Uppsala University, Uppsala, Sweden. [3] Department of Surgical Sciences, Plastic Surgery, Uppsala University, Uppsala, Sweden.

Alternatively, the microwave based sensors developed in [1, 6] have been shown remarkably promising. The microwave sensor can be designed in handheld size for portability; therefore, it can be used in hospital and at home. For safety aspects, the microwave sensor radiates non-ionizing energy, so it is suitable for infants to be measured for multiple times to have follow-up after craniotomy [1–6]. In [1], the compact split ring resonator (SRR) was realized for monitoring the healing stages. An open ended circular waveguide antenna was proposed in [6] to investigate the impedance changes with respect to healing stages. In this paper, we have presented the preliminary research of monitoring the healing stages utilizing a short pulsed radar technique. The paper is organized as follows. The resistively loaded dipole antenna and its performance are introduced in Section 2.1. The developed microwave phantoms are presented in Section 2.2. In Section 3, the longitudinal scan measurement result and the concept of one-dimensional pulsed profile are provided. The conclusion of this paper is finally given in Section 4.

2. MATERIALS

2.1. Resistively-Loaded Dipole Antenna

The resistively loaded dipole antenna as shown in Fig. 1 is designed using Ansys HFSS simulator [7]. The antenna with a dimension of 95 mm × 50 mm was realized on an FR-4 substrate of 0.8 mm thickness ($\varepsilon_r = 4.4$, $\tan\delta = 0.02$). The five resistors are separated in a row and are placed between the strip lines in an effective manner. A triangular tapered balun was designed using microstrip and parallel strip line to convert unbalanced structure to balanced one. As shown in Fig. 2(a), the scattering parameters of measurement and simulation are compared. The measurement result of transmission coefficient curve is in good agreement with simulation result, whereas the discrepancy between measurement and simulation of reflection coefficient curve at higher frequency is observed. The matching chip resistor cannot cover

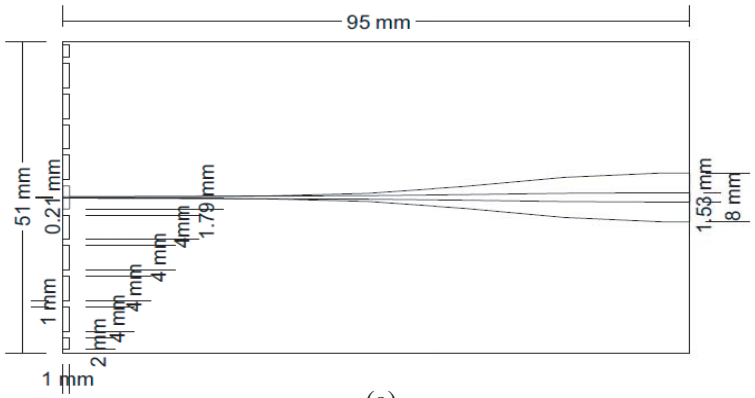

(a)

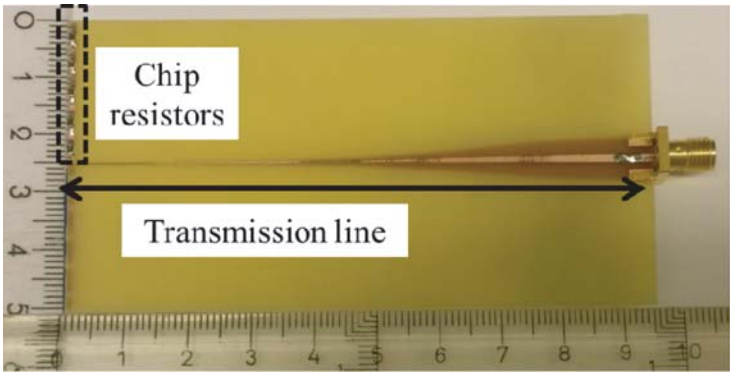

(b)

Figure 1. Proposed resistively loaded dipole antenna. (a) Schematic of antenna. (b) Fabricated antenna.

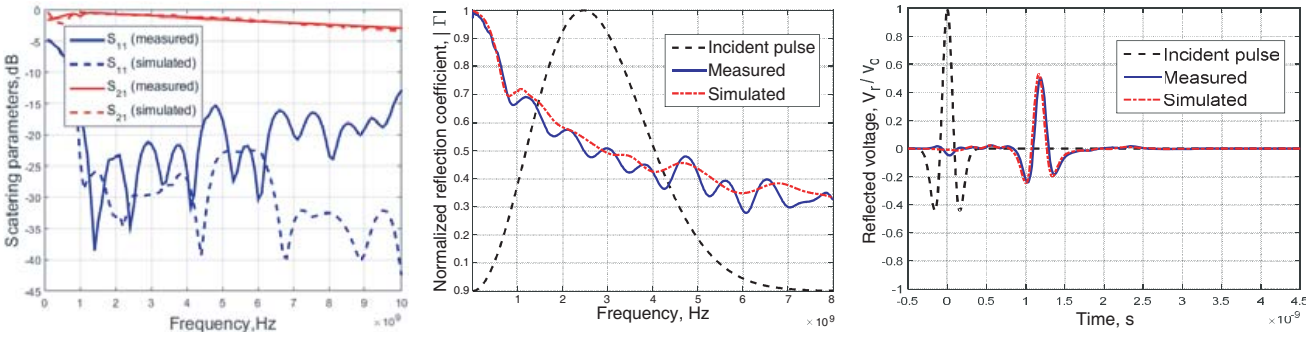

(a) (b) (c)

Figure 2. Performance of resistively loaded dipole antenna [3]. (a) Scattering parameters of fabricated balun. (b) Normalized reflection coefficient curve. (c) Reflected pulse of antenna in time domain.

the higher frequency region (100 MHz to 5 GHz).

The antenna is loaded with chip resistors on both sides of the arms to effectively suppress the reflection from open-end arms. In this way, the loaded resistors make the antenna bandwidth broad. The loaded chip resistors can be determined by integrating the segments of the Wu-King resistive profile, in which the antenna arm is normalized by resistance per unit length [8]. The calculated chip resistors are then 115 Ω, 150 Ω, 210 Ω, 348 Ω, 1 KΩ. As shown in Fig. 2(b), the reflection coefficient curve shows a non-resonance pattern, but traveling pattern over wide band when a second derivative Gaussian pulse is excited.

Figure 2(c) shows the reflected pulse in time domain. The simulated and measured curves are in good agreement. There is a port reflection around 0 s. The balun reflection is then observed until 1.25 ns. The reflected pulse waveform is very clear that is a replication of incident pulse. This results in radiating the pulse without antenna's own distortion. This characteristic is pretty desirable for sensing small skull defect response in this work.

2.2. Microwave Head Phantom Development

The tissue mimicking phantoms were developed for simulating the interaction between physiological changes in defect area and reflection from defect area. We have considered agar based phantoms because agar has the ability to preserve the water contained mixture as well described in [3, 4, 9]. The pure deionized water was utilized to make sure that the mixture is not affected by any chemical ions. The sodium chloride (Jozo fine salt, Sweden) was employed to control the conductivity of phantom. The agar (Nice Chemicals Pvt Ltd., Kerala, India) was a main material to have the mixture to be shaped. Polyethylene powder (PEP, Seishin Enterprose Co., Japan) was mixed to adjust the real part of relative permittivity of mixtures. Here, we added the TX-151 (Balmar, LLC, Louisiana, USA) to improve the viscosity of mixtures because the agar and PEP cannot mix properly with each other. To make each tissue a homogeneous media, we considered the volumetric fraction of all tissues to reflect the multi tissue layers as one layer [3]. Each material of tissue mimicking phantoms was followed as shown in Table 1 to adjust the electrical properties of phantoms as similar to the reference, which is available in [10]. All fabricated phantoms were evaluated using a 200 mm long open-ended slim probe (Agilent 85070E) for 1 GHz to 6 GHz.

Figure 3 shows the measured electrical properties such as dielectric permittivity and conductivity as a function of frequency. We developed the tissue mimicking phantoms for 1 GHz to 6 GHz where this ranges are optimized for antenna performance. The theoretical curves of all tissues are calculated using numerical equation which is available in [10]. The measured curves are in a good agreement with theoretical ones.

Table 1. Component configuration of tissue mimicking phantoms [3].

Tissue based on mass [g]/[100g D.I.]	PEP [25 µm]	Calcium sulfate	Sodium chloride	TX-151	Agar
Brain	16.52		1.13	2.54	3.12
Skull	35	150	0.6	0.6	
Skin	21.24		0.52	1.344	3.12

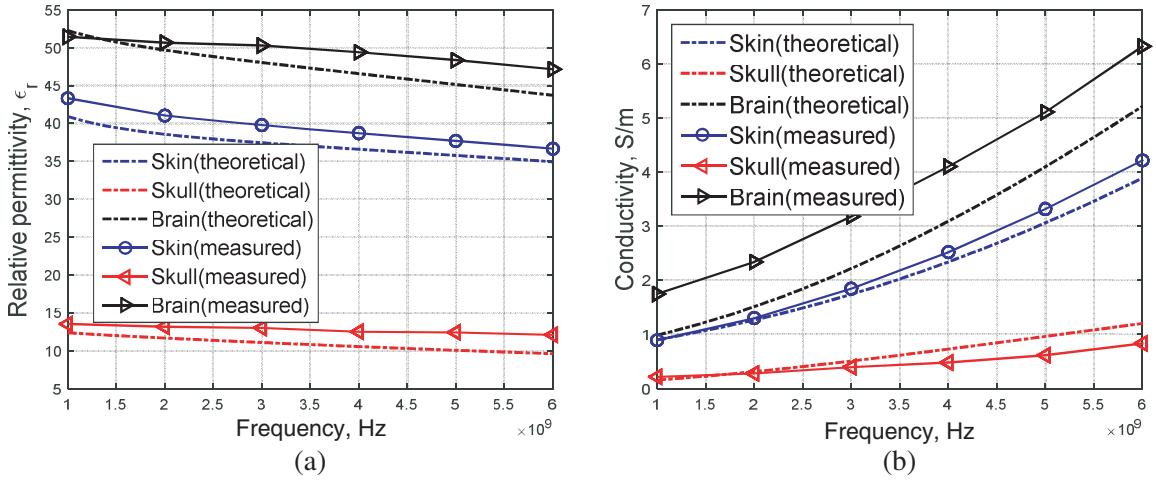

Figure 3. Measured electrical properties of fabricated tissue mimicking phantoms [3]. (a) Relative permittivity. (b) Conductivity.

3. IMPLEMENTATION

3.1. Experimental Setup and Calibration Process

The layered cranial surgery phantom model such as skin, skull, and brain layer was developed as a preliminary study as shown in Fig. 4. We created a void inside the skull layer as part of representing the craniotomy defect. The void size is comparable with the reference available in [11]. The skull powder in void was then stacked up for emulating the healing progression such as 1 mm, 3 mm, 5 mm, 7 mm, and 10 mm. Here, we investigated the reflection from every healing stage. The measurement was carried out using PNA E8364B. The reflection coefficient of all healing stages was measured from 0.1 GHz to 8 GHz with 100 MHz step size.

The calibration process is proposed to make the defect response more visible than other reflections. The proposed process is as follows:

$$v_{cal}(t) = IFFT\left[\left\{S_{11,w/}(f) - S_{11,w/o}(f)\right\} \times FFT\left\{v_{in}(t)\right\}\right] \tag{1}$$

where $v_{cal}(t)$ is calibrated reflected voltage; $S_{11,w/}(f)$ is measured reflection coefficient with skull powder environment; $S_{11,w/o}(f)$ is measured reflection coefficient without skull powder environment; IFFT and FFT are Inverse Fast Fourier Transform and Fourier Transform; $v_{in}(t)$ is incident pulse which is generated in MATLAB as follows [12]:

$$v_{in}(t) = -t/\tau_p \cdot \exp\left(1/2 - t^2/2\tau_p^2\right) \tag{2}$$

where τ_p is the characteristic parameter of differentiated Gaussian pulse which is related to pulse width such as:

$$\tau_p = 1/2\pi f_{peak} \tag{3}$$

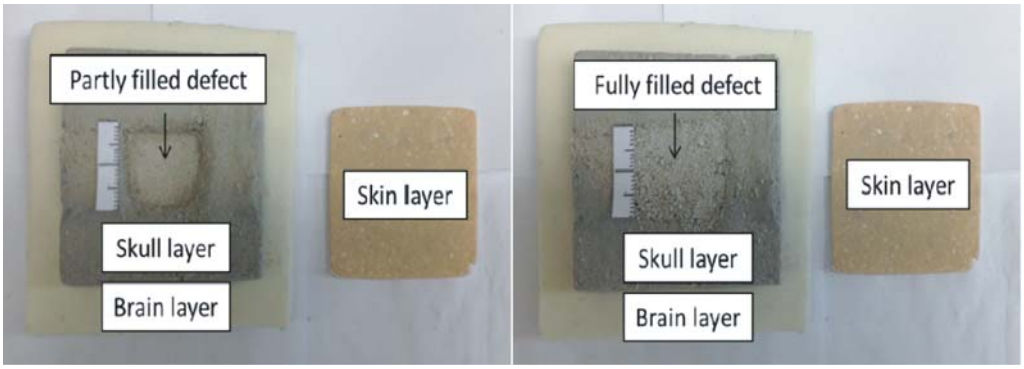

Figure 4. Layered cranial surgery phantom models; skull powder is stacked inside the void in skull layer to emulate the surgical area.

where f_{peak} is the peak frequency of the incident spectrum which was determined at 2.5 GHz where the width of pulse should be narrower than the time required for waves to travel the length of skull layer.

The $S_{11,w/o}(f)$ measurement can be considered as right immediately after craniotomy because there will be an empty space in defect area. $S_{11,w/}(f)$ can also be considered as every healing stage measurement in reality. The calibrated reflected voltage can then be obtained from subtracting captured $S_{11,w/o}(f)$ measurement from every measured $S_{11,w/}(f)$ data. In this procedure, we investigated the healing stages using calibrated reflected voltage as a preliminary study.

3.2. Longitudinal Scan

The longitudinal scan of various thicknesses was carried out to explore the healing progression as a preliminary study. The distance between antenna and phantom was determined by 75 mm where it is in vicinity of the defect because there is a high loss in air medium. Figs. 5(a)–5(f) show the measurement result for various thicknesses of skull powder. We controlled the thickness of skull as powdered skull phantom such as 1 mm, 3 mm, 5 mm, 7 mm, and 10 mm to emulate the progression of healing stages. Around 1.25 ns, there is an antenna reflection, which is highlighted by subtracting two voltages (one is for reflection coefficient with skull powder environment and the other for reflection coefficient without skull powder environment). The defect response is then observed at around 1.75 ns for all thicknesses. Here, it is clearly observed that the amplitude of reflection is increased as thickness of skull powder is increased. This is because the reflection strongly depends on the effective dielectric properties of defect area which is on the composition of the defect cavity [13, 14]. We believe that the tail ringing after defect response observed is due to multiple reflections from layers. We can conclude that the amplitude variation of reflected voltage could be an indicator of progression of healing stages.

The craniotomy defect created as a part of craniosynostosis treatment is a dynamic scenario in reality. This is because the subjects are newborn and have high bone regeneration rates. The defect goes through physiological changes such as an inflammation and deposition of bone minerals. These changes provide very high temporal contrast between various healing stages of skull defect area. Therefore, tracking the healing process using radar based technique is rather straightforward.

3.3. One-Dimensional Pulsed Profile

The one-dimensional pulsed profile was obtained for achieving the pulse compression so that the defect response can be highlighted. The overall signal processing of one-dimensional pulsed profile is presented in Fig. 6. The source is generated and transmitted toward defect area. The defect reflection is then received. After that, down conversion is processed for moving frequency to base band. Then, the matched filter is applied using a reference pulse. The detailed signal processing is shown in Figs. 7(a)–(f). Here, the linear frequency modulated pulse, up-chirp pulse, is generated in MATLAB as a source

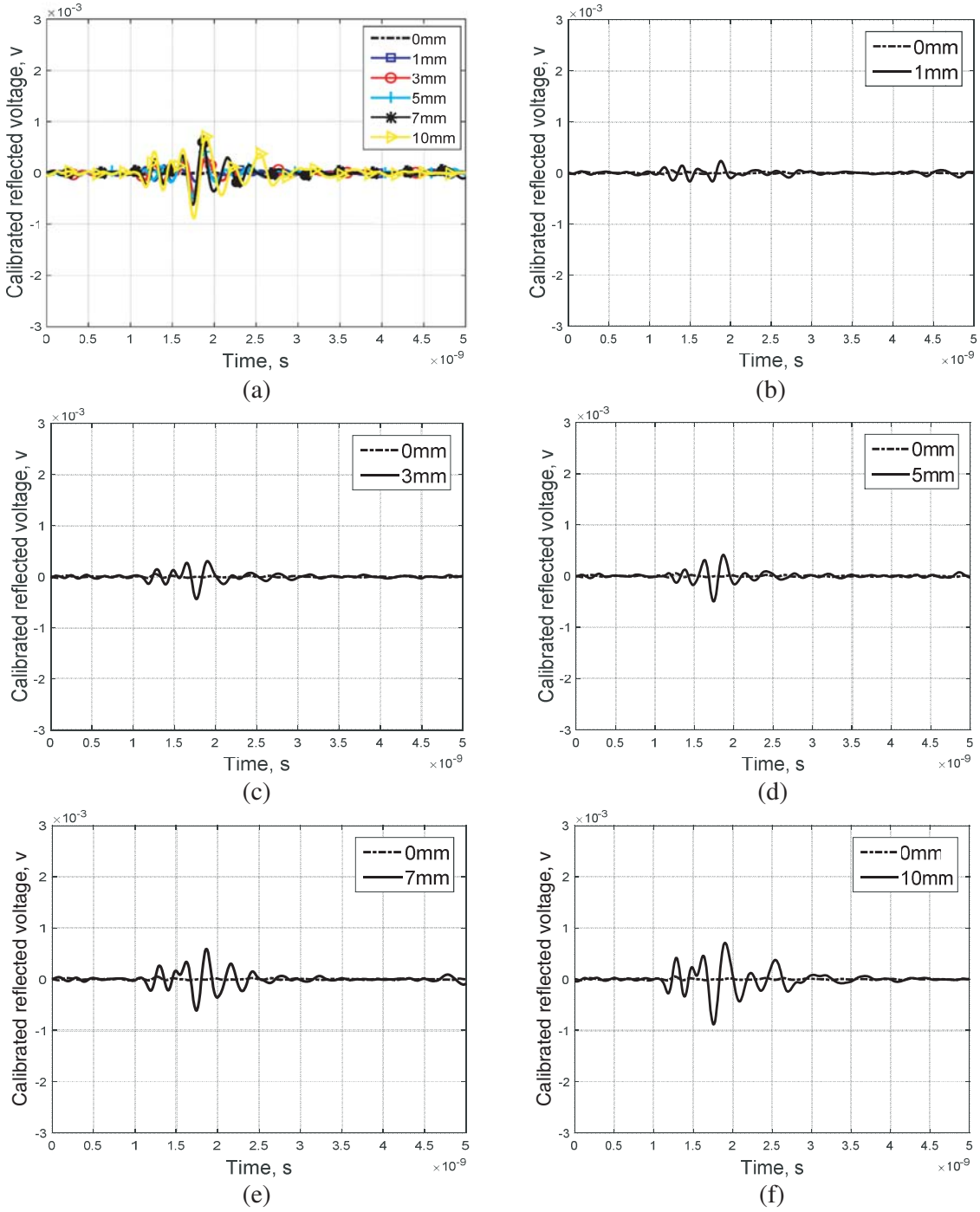

Figure 5. Calibrated reflected voltage of defect thicknesses. (a) All thicknesses. (b) 1 mm. (c) 3 mm. (d) 5 mm. (e) 7 mm. (f) 10 mm.

shown in Fig. 7(a) which can be expressed as follows:

$$v_{in}(t) = \begin{cases} \exp\left\{j2\pi\left(f_0 t + K \cdot t^2/2\right)\right\}, & |t| \leq T_1/2 \\ 0, & \text{elsewhere} \end{cases} \tag{4}$$

where f_0 is the starting frequency of 1 GHz, K the chirp rate, and T_1 the pulse duration of 4 ns. The chirp pulse is characterized by 5 GHz bandwidth where the antenna is properly working this range. For

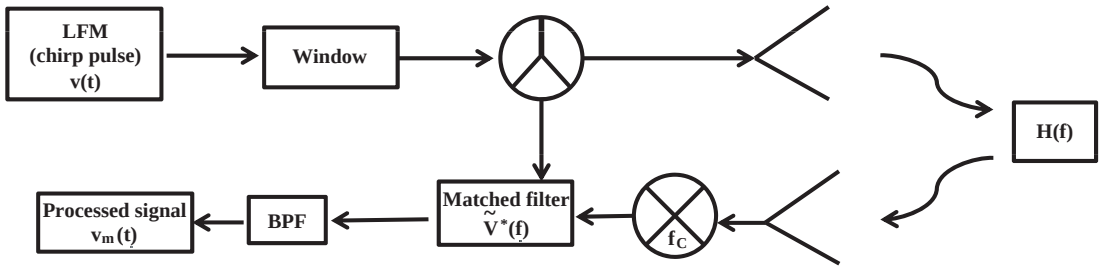

Figure 6. Block diagram of signal processing for achieving one-dimensional pulsed profile.

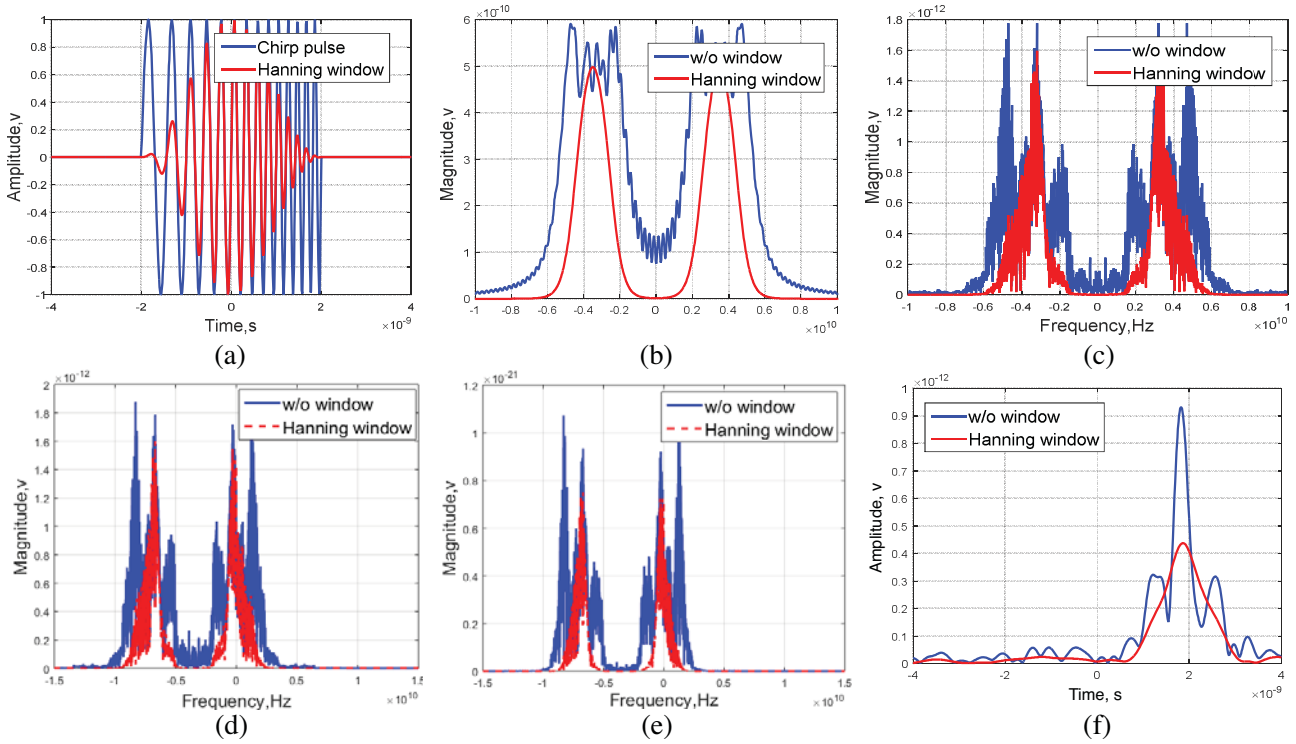

Figure 7. Signal processing of one-dimensional pusled profile for measured raw data of 10 mm skull powder case. (a) Up chirp pulse in time domain. (b) Chirp spectrum. (c) Received spectrum. (d) Down conversion processing. (e) Matched filter response in frequency domain. (f) Matched filter response in time domain.

sudden changes in chirp pulse at the beginning and end of the time, it eventually results in side peaks in time domain as shown in Fig. 7(f). Also, the antenna does not radiate the DC component; therefore, it should be suppressed for a proper operation. In this respect, we applied the Hanning window to have a smooth curve in time domain and reduce the DC component in frequency domain as shown in Fig. 7(b). As introduced in Section 3.2, the reflected pulse is then received for every healing stage as shown in Fig. 7(c). The center frequency is down toward base band to proceed further signal processing as shown in Fig. 7(d). Here, the matched filter is applied to correlate and highlight the defect reflection such as:

$$\tilde{V_m}(f) = \tilde{V_{rx}}(f) \cdot \tilde{V_{ref}^*}(f) = \tilde{S_{11}}(f) \cdot \tilde{V_{in}}(f) \cdot \tilde{V_{in}^*}(f) = \tilde{S_{11}}(f) \cdot \left|\tilde{V_{in}}(f)\right|^2 \tag{5}$$

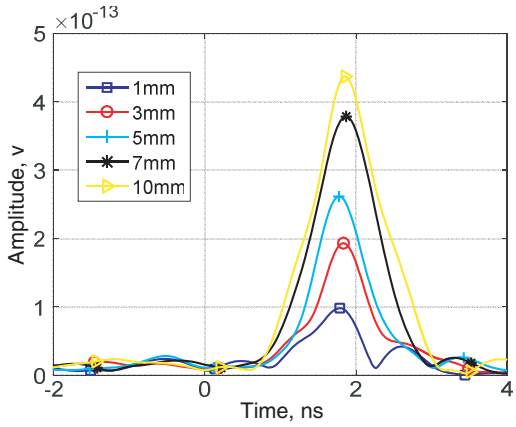

Figure 8. Matched filter response for all thickness cases.

where $\tilde{V_m}(f)$ is the processed matched filter response, $\tilde{V_{rx}}(f)$ the received pulse, and $\tilde{V}^*_{ref}(f)$ the complex conjugate of the reference pulse for the correlation process. Here, we used the chirp source, $\tilde{V_{in}}(f)$, as the reference pulse. In this way, the matched filter response can follow the defect reflection as shown in Eq. (5). The processed matched filter response can finally take an envelope of reflected pulse as shown in Fig. 7(f). It can be observed, with applied Hanning window, that the side peak in time domain as shown in Fig. 7(f) is reduced at the expense of the reduced amplitude of reflection. The highlighted defect response together with reduced side peak is very desirable for this study. The final matched filter response for all thickness cases is stacked as shown in Fig. 8.

4. CONCLUSION

A resistively loaded dipole antenna has been proposed and characterized in this study. The antenna was analyzed on layered head phantom models as a preliminary study to use it in longitudinal sensing of the reflection of the effective dielectric constant of skull defect area after open skull surgery. The imaging setup has been used to monitor the changes in the physiology which has a strong dependence with effective dielectric constant in the skull defect area during various healing stages. It enables this technique to keep a track on the very critical skull healing in newborn more frequently without any radiation hazards. To the best of our knowledge, it is a potential technique to explore the skull healing progression using the principle of short-pulsed radar technique. The current studies have been carried out on flat homogenous phantoms, but more radar experiments with due consideration of skull curvature will be carried out in the future.

ACKNOWLEDGMENT

This work was supported by the Vinnova and Swedish Research Agency, Vetenskapprådet Sweden.

REFERENCES

1. Raman, S., R. Augustine, and A. Rydberg, "Non-invasive osseointegration analysis of skull implants with proximity coupled split ring resonator antenna," *IEEE Trans. Antennas Propag.*, Vol. 62, No. 11, 5431–5436, Nov. 2014.
2. Raman, S., R. Augustine, and A. Rydberg, "Geometrical and dimensional dependance of skull implants on oseointegration analysis using microwave probe," *IEEE Conference on Antenna Measurements & Application (CAMA)*, 1–4, Nov. 2014.
3. Lee, D., D. Nowinski, and R. Augustine, "A UWB sensor based on resistively-loaded dipole antenna for skull healing on cranial surgery phantom models," *Microw. Opt. Technol. Lett.*, Vol. 60, 897–905, 2018.

4. Augustine, R., S. Raman, and A. Rydberg, "Microwave phantoms for craniotomy follow-up probe," *IEEE Conference on Antenna Measurements & Applications (CAMA)*, 1–2, Nov. 2014.
5. Akram, S. B. S., N. Qaddoumi, and H. Al-Nashash, "Novel near-field microwave bone healing monitoring using open-ended rectangular waveguides," *2006 IEEE GCC Conference (GCC)*, Manama, 1–5, 2006.
6. Mathur, P., D. G. Kurup, and R. Augustine, "Design of open ended circular waveguide for non-invasive monitoring of cranial healing in pediatric craniosynostosis," *2017 First IEEE MTT-S International Microwave Bio Conference (IMBIOC)*, 1–4, 2017.
7. Ansoft HFSS, available online at http://www.ansoft.com/prouct/hf/hfss.
8. Wu, T. T. and R. W. P. King, "The cylindrical antenna with nonreflecting resistive loading," *IEEE Trans. Antennas Propag.*, Vol. 13, No. 3, 369–373, May 1965.
9. Okano, Y., K. Ito, and H. Kawai, "Solid phantom composed of glycerin and its application to SAR estimation," *IEICE Trans. Commun.*, 534–543, 2000.
10. Andreuccetti, D., R. Fossi, and C. Petrucci, "An internet resource for the calculation of the dielectric properties of body tissues in the frequencyrange 10 Hz–100 GHz," Website at http://niremf.ifac.cnr.it/tissprop/, IFAC-CNR, Florence, Italy, 1997.
11. Teng, C.-C., L. G. Shapiro, R. A. Hopper, and J. V. Halen, "Pediatric cranial defect surface analysis for craniosynostosis postoperation ct images," *5th IEEE International Symposium on Biomedical Imaging: From Nano to Macro*, 620–623, Paris, France, May 14–17, 2008.
12. The MathWorks, available online at http://www.mathworks.com/.
13. Augustine, R., D. G. Kurup, S. Raman, D. Lee, K. Kim, and A. Rydberg, "Bone mineral density analysis using ultra-wideband microwave measurements," *2015 IEEE MTT-S International Microwave and RF Conference (IMaRC)*, 102–104, Hyderabad, 2015.
14. Augustine, R., D. G. Kurup, S. Redzwan, P. Mathur, S. Raman, D. Lee, and K. Kim, "Microwave reflectivity analysis of bone mineral density using ultra-wide band antenna," *Microw. Opt. Technol. Lett.*, Vol. 59, 21–26, 2017.